Bound entanglement in symmetric random induced states

J. Louvet [*], F. Damanet [†] and T. Bastin [‡]
Institut de Physique Nucléaire, Atomique et de Spectroscopie, CESAM, University of Liège, B-4000 Liège, Belgium

(Received 19 November 2025; accepted 19 March 2026; published 16 April 2026)

Bound entanglement, a weak, yet resourceful, form of quantum entanglement, remains notoriously hard to detect and construct. We address this here by leveraging symmetric random induced states, where positive partial transpose (PPT) bound entanglement arises naturally under partial tracing when proper parameters are selected. We investigate the probability of finding PPT bound entanglement in symmetric random induced states constructed via two methods: partial tracing of symmetric multiqubit pure states, on the one hand, and tracing out a qudit ancilla, on the other hand. For $N > 3$ qubits, we demonstrate that bound entanglement naturally emerges under optimal parameters, with a probability of occurrence very close to 1. We show that the two methods produce different varieties of PPT bound entangled states and identify the contexts in which each method offers distinct advantages. These methods provide a versatile toolkit for the generation of large families of random PPT bound entangled states without complex numerical optimization.

DOI: 10.1103/klk3-wjvn

I. INTRODUCTION

Since its discovery, quantum entanglement has been regarded as the most nonclassical characteristic of quantum mechanics. Over the decades, extensive research efforts have been dedicated to the detection, characterization, and manipulation of quantum entanglement, which constitutes a pivotal resource for quantum sciences and technologies [1,2]. Despite these efforts, determining whether a multipartite state is separable or entangled, a challenge known as the separability problem [1], remains daunting in the most general scenario. For qubit-qubit and qubit-qutrit systems, there exists a straightforward necessary and sufficient condition to address this problem [3,4]. However, for systems in higher dimensions, the development of efficient analytical or numerical methods to solve the separability problem remain challenging. This difficulty is partially attributed to a form of entanglement that poses significant detection challenges, known as bound entanglement, which gathers all those states that are entangled but are not distillable, i.e., from which no pure maximally entangled pairs can be extracted using local operations and classical communication [5]. The utility of these states has been demonstrated across various applications, including the conversion of pure entangled states [6], quantum key distribution [7], and quantum metrology [8,9]. Nonetheless, constructing such states remains a nontrivial task, given the incomplete characterization of the set of bound entangled states. The first bound entangled states were presented in [5,10], along with a family of states for which bound entanglement can be activated [11]. The subsequent analytical construction of bound entangled states primarily employed unextendible product bases [12–15], and constructions of bound entangled states from existing ones have also been explored [16,17]. Prior work showed that bound entangled states can also be generated through Lorentz boosts [18]. Numerous other analytical and numerical approaches have been investigated to construct bound entangled states [19–33], but no straightforward efficient way to generate large families of bound entangled states has been investigated.

In this paper, we show how one can obtain bound entangled states within symmetric random induced states (RIS). A RIS is obtained by tracing out an ancillary system from an initial random pure state of the global system. Recent findings indicate that bipartite bound entanglement can be generically obtained in RIS for systems of sufficiently large dimensions [34]. However, the question remains to be studied and clarified for low dimensions. The present study addresses this gap by examining the efficiency of obtaining bound entanglement in multipartite N-qubit systems in symmetric RIS for low to moderate N values. We study two distinct constructions that successfully generate bound entanglement with different properties. Since the only operation involved in generating random induced states is the partial tracing over an ancillary system, our methods provide straightforward access to symmetric multipartite bound entangled states.

The paper is organized as follows. In Sec. II, we first present the necessary background and definitions related to entanglement, bound entanglement, symmetric states, and RIS. In Sec. III, we describe the two methods used for constructing bound entangled RIS states. In Sec. IV, we present the results for both methods and compare them. Finally, in Sec. V, we conclude and provide several perspectives on our work.

II. BACKGROUND

A. Bound entanglement

Entangled states ρ are states that cannot be expressed as a convex combination of separable product states [1,2].

[*]Contact author: jlouvet@uliege.be
[†]Contact author: fdamanet@uliege.be
[‡]Contact author: T.Bastin@uliege.be

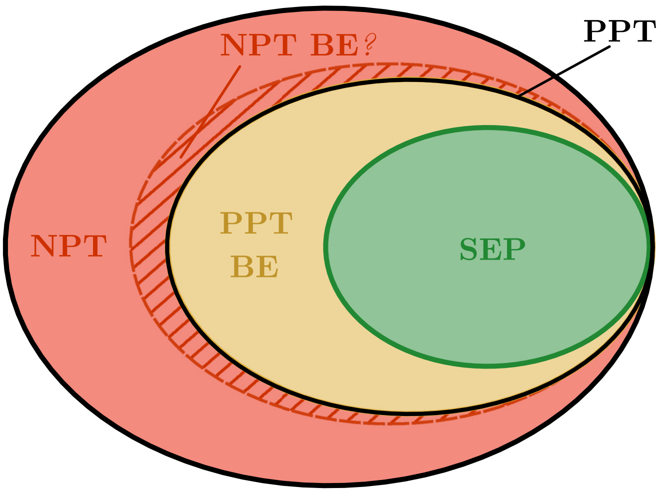

FIG. 1. Set of bipartite states. Separable states (SEP), PPT BE, and NPT entangled states (NPT). The union of the PPT BE and SEP states yield all PPT states. It is still an open question whether there exists NPT bound entangled states (NPT BE) [35]. For 2×2 and 2×3 systems, the PPT BE set is empty [3,4].

The Peres-Horodecki positive partial transpose criterion (PPT criterion) provides a straightforward, sufficient condition for entanglement: a quantum state ρ is entangled across the bipartition $A|B$ if its partial transposition ρ^{T_A} has at least one negative eigenvalue. This criterion is necessary and sufficient for qubit-qubit and qubit-qutrit systems [3,4]. In higher dimensions, PPT states, i.e., states with a positive partial transpose, may still exhibit entanglement. PPT entangled states have the property that they cannot be distilled [5]. The entanglement in nondistillable states is *bound* to the state, hence their name: Bound entangled (BE) states. By contrast, the question of whether the entanglement of all negative partial transpose (NPT) states can be distilled remains open [35]. Figure 1 summarizes the different entanglement properties of bipartite states. Throughout this work, bound entangled states will refer to PPT BE states. In the context of multipartite systems, quantum states can be entangled with regard to (w.r.t.) some bipartitions while not w.r.t. others, and the same applies for the PPT property. States that are PPT and entangled w.r.t. a given bipartition are bound entangled w.r.t. this bipartition. To fully characterize a multipartite state, one thus has to go over every possible bipartition of the system, see, e.g., [26].

B. Symmetric N-qubit states

Multipartite symmetric states are states that remain invariant under any permutation of their parties. Symmetric N-qubit states live in the symmetric subspace $\mathcal{H}_S$ of dimension $N+1$. It is spanned by the Dicke states

$$|D_N^\alpha\rangle = \binom{N}{\alpha}^{-1/2} \sum_\sigma P_\sigma |\underbrace{0\ldots0}_{N-\alpha}\underbrace{1\ldots1}_{\alpha}\rangle \qquad (1)$$

for $\alpha = 0, \ldots, N$, where the sum runs over all possible permutation operators P_σ of the N qubits. Two major simplifications emerge when investigating the entanglement of symmetric states. First, for symmetry reasons, a symmetric state can only be either separable across all possible bipartitions or across none. In the first case the state is said to be fully separable, in the latter the state it is entangled across all possible bipartitions and said to be genuinely multipartite entangled [2]. Second, while a symmetric state can be PPT w.r.t. some bipartitions and not w.r.t. others (so that symmetric states can be PPT bound entangled only w.r.t. specific bipartitions), only the number of qubits in each part of the bipartitions is relevant since any permutation of the qubits leaves the state unchanged. Therefore, the bipartitions $A|B$ can be merely denoted by their cardinalities, and an entangled symmetric state of N qubits can only be PPT bound entangled across any of the bipartitions $N-1|1, N-2|2, \ldots, \lceil N/2\rceil|\lfloor N/2\rfloor$.

C. Random induced states

A RIS on $\mathcal{H}^d$, where d denotes the dimension of the state space $\mathcal{H}$, is defined as a mixed state obtained after adding an ancilla to the system and partially tracing a random pure state on the enlarged space $\mathcal{H}^d \otimes \mathcal{H}_a^{d_a}$ over the ancilla degrees of freedom, where $\mathcal{H}_a^{d_a}$ is the ancilla state space of dimension d_a. If the system state space $\mathcal{H}^d$ can be evenly bipartitioned as $\mathcal{H}^{d/2} \otimes \mathcal{H}^{d/2}$, it is demonstrated that, for large dimensions d, the probability of obtaining an entangled RIS is high, as long as the ancilla state space dimension d_a is smaller than some threshold s [34]. Similarly, the probability of obtaining a PPT RIS is high as long as d_a is greater than some other threshold $p < s$ [36]. In between these two thresholds (for $p < d_a < s$), there is a high probability that the RIS is PPT entangled. While the arguments presented are also valid for unbalanced bipartitions, it is unknown if there exists such thresholds for low dimensions d or if a region of PPT entangled states exists. These studies also leave the entanglement properties of random induced states in the symmetric subspace unexplored. Here, we fill in these gaps.

III. METHODS

In this section, we present the two methods investigated to generate symmetric random induced states, as well as the method we employ to detect bound entanglement and how we estimate the probability to get bound entanglement in the RIS.

A. Generation of RIS

We consider two different methods to generate random induced states.

(1) *Method I (MI)*. We generate a random $(N+N_a)$-qubit symmetric pure state $|\psi_1\rangle$ on $\mathcal{H}_S^{N+N_a+1}$ and trace out N_a qubits, i.e., the RIS is given by $\rho_1 = \mathrm{Tr}_{N_a}(|\psi_1\rangle\langle\psi_1|)$.

(2) *Method II (MII)*. We generate a random pure state $|\psi_2\rangle$ on $\mathcal{H}_S^{N+1} \otimes \mathcal{H}_a^{d_a}$ and trace out the qudit ancilla system $\mathcal{H}_a^{d_a}$ of dimension d_a, i.e., the RIS is given by $\rho_2 = \mathrm{Tr}_a(|\psi_2\rangle\langle\psi_2|)$.

In both methods, the generated RIS ρ are symmetric, i.e., $P_\sigma\rho = \rho = \rho P_\sigma$, for all permutations σ of the N qubits. For both cases, the initial random pure states $|\psi_1\rangle$ and $|\psi_2\rangle$ are generated according to the unitarily invariant Fubini-study measure in the space of pure states (the Haar measure), which ensures that all random pure states on $\mathcal{H}_S^{N+N_a+1}$ and $\mathcal{H}_S^{N+1} \otimes \mathcal{H}_a^{d_a}$ are generated equiprobably [37]. Figure 2 illustrates both methods.

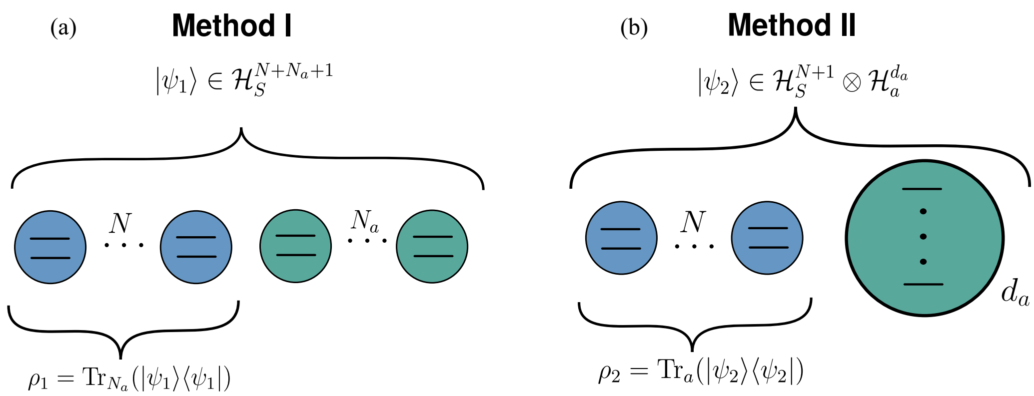

FIG. 2. Generation of RIS. Method I (a): A RIS ρ_1 is created from an initial pure state $|\psi_1\rangle$ randomly generated on the symmetric subspace $\mathcal{H}_S^{N+N_a+1}$ of $N + N_a$ qubits after tracing out N_a qubits. Method II (b): A RIS ρ_2 is created from an initial pure state $|\psi_2\rangle$ randomly generated on the tensor product space $\mathcal{H}_S^{N+1} \otimes \mathcal{H}_a^{d_a}$ of the symmetric subspace of N qubits and a d_a-dimensional qudit after tracing out the ancilla qudit.

B. Detection of PPT bound entanglement

To assess whether the generated RIS is NPT, PPT BE, or SEP, we check if the state is PPT across the different bipartition of the N qubits. Since the RIS is symmetric, as soon as one of its bipartitions is NPT, the state is necessarily genuinely entangled, i.e., entangled accross every bipartition. If the state is in contrast PPT accross every bipartition, the separability problem must be solved to assess or not the full separability of the state. To do so, we use the reformulation of the separability problem as a truncated moment problem that we solve using semi-definite optimization [38], as it is very efficient for symmetric qubits. The different outcomes are then the following.

(1) *NPT*. The state is NPT for every bipartition. There is NPT entanglement across all partitions.

(2) *PPT BE*. The state is PPT for at least one bipartition and NPT for the others. There is PPT bound entanglement across the PPT bipartitions.

(3) *SEP*. The state is PPT for every bipartition and is fully separable.

It may happen that in some cases the separability problem is unresolved with this method. These cases are tracked in our process and tagged UNK for unknown states. Note that for $N = 2$ and $N = 3$, the only bipartitions are $1|1$ and $2|1$, respectively. For these dimensions, PPT states are also separable by the PPT criterion, thus PPT bound entangled bipartitions can then arise for $N > 3$ [3,4].

C. Estimation of the probabilities

The probability P_{K} (K = NPT, PPT BE, SEP) of obtaining NPT, PPT BE, and SEP states, respectively, using either method I or II is given by

$$P_{\mathrm{K}} = \lim_{n\to\infty} \frac{n_{\mathrm{K}}}{n}, \tag{2}$$

with n_{K} the number of times a K state is found among the set of n RIS using the respective methods. We similarly define the probability P_{UNK} that methods MI and MII generate a PPT RIS that cannot be detected as either separable or entangled by our implementation of the truncated moment reformulation of the separability problem.

The probabilities P_{K} are estimated by using the empirical probabilities $\tilde{P}_{\mathrm{K}}(n) = n_K/n$ for a fixed number n of RIS. For large n, $P_{\mathrm{K}} \simeq \tilde{P}_{\mathrm{K}}(n)$. The validity of this approximation is analyzed through the convergence of $\tilde{P}_{\mathrm{K}}(n)$ with respect to n. We conclude that with $n = 10^5$ the approximation is expected to hold within a precision of 10^{-3} (see Appendix).

IV. RESULTS

This section presents our results about the probabilities of generating PPT BE states, as well as NPT and SEP states, from the two kinds of RIS generated in this paper. We show how they scale with system size N. We also provide a discussion about the different properties of the obtained PPT BE states depending on the methods used to generate the RIS, and compare the two methods.

A. Probabilities

As shown in Figs. 3 and 4, it is possible to create bound entanglement in symmetric N-qubit RIS with both methods MI and MII as soon as $N > 3$. Upon increasing the ancilla parameters N_a and d_a, we observe three distinct entanglement "phases." First, the probability to obtain an NPT RIS starts from a maximal value 1 (to within 10^{-3}), then decreases down to 0, while the probability of obtaining a PPT BE state increases to reach a maximum inbetween. The maximum PPT BE probability varies and increases with N in MI for $N = 4, 5, 6$ and in MII for $N = 4, 5$, reaching a value close to 1 in both methods for higher N. This probability then decreases down to 0, while the probability of obtaining a fully separable RIS increases and tends to 1. This behavior aligns with the analytical results reported in [34,36] for large dimensions in the bipartite scenario. However, here we do not observe sharp thresholds between the different phases. The increase (or decrease) in each probability is not abrupt, but rather gradual.

Let us focus on the PPT BE RIS (the yellow curves on Figs. 3 and 4). The notation PPT $\mathrm{BE}_{k_1,\ldots,k_J}$ denotes PPT bound entanglement across all the bipartitions $N - k_j|k_j$ ($j = 1, \ldots, J$). In case the state is PPT bound entangled across all possible bipartitions (all possible bipartitions but the

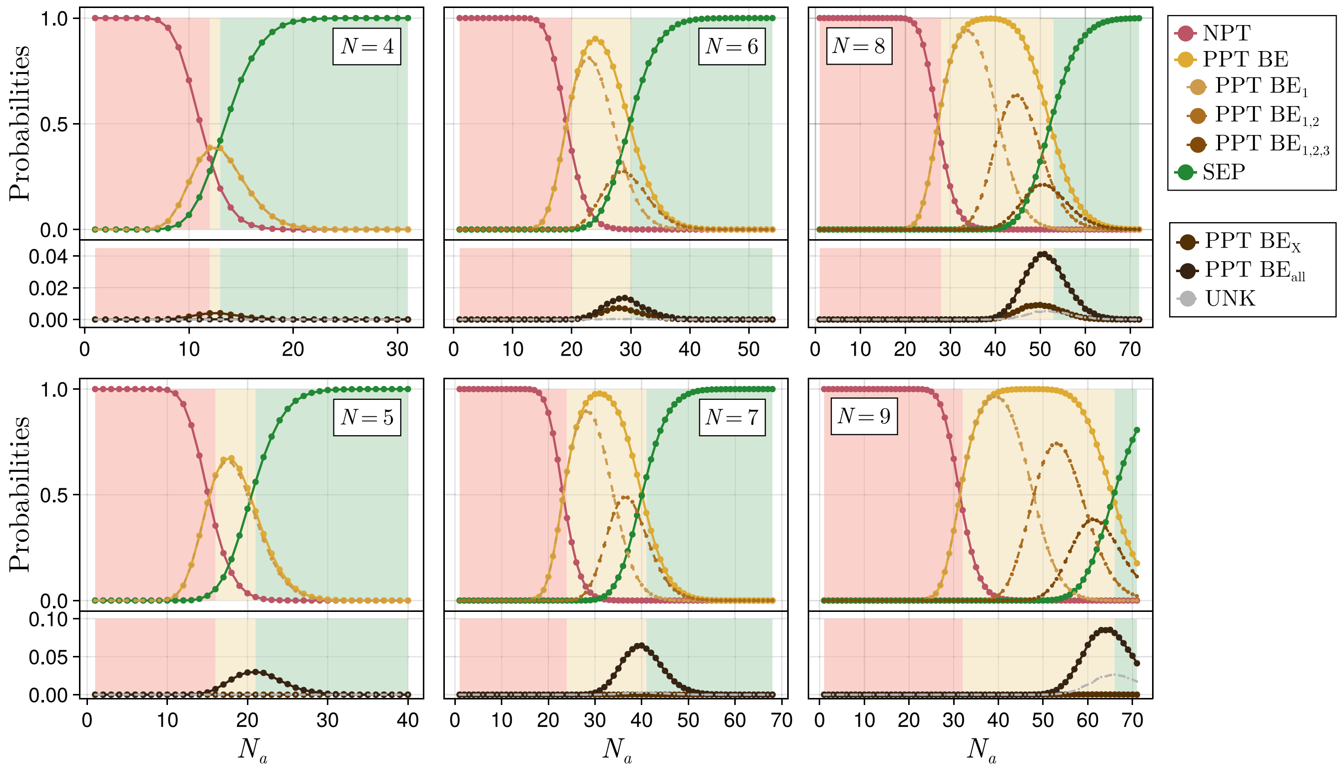

FIG. 3. Bound entanglement in Method I. Probabilities that the generated random induced states have NPT entanglement (red), PPT bound entanglement (yellow), or are separable (green) using Method I with respect to the number of qubits N_a in the ancilla system, for $N = 4, \ldots, 9$. N_a starts at 1 and increases with a step of 1. The maximal PPT BE probability quickly grows to 1 as N increases, showing the efficiency of the method. The brown curves are a refinement of the PPT BE yellow curve. They show the probabilities of obtaining PPT bound entanglement across the different bipartitions: PPT BE$_1$, PPT BE$_{1,2}$, and PPT BE$_{1,2,3}$ as the ancilla parameter increases. The PPT BE$_1$ curve and the global PPT BE curve (yellow) are almost identical for $N = 4$ and 5. The bottom frame exhibit the three probabilities of getting PPT BE$_X$, PPT BE$_{all}$, and UNK states. The lines between the dotted points are to guide the eye. The background colors indicate the regions where the probability of obtaining NPT entanglement (red), PPT bound entanglement (yellow), or separable states (green) is the highest compared to the other two.

penultimate $\lceil N/2 \rceil + 1 | \lfloor N/2 \rfloor - 1$), it is also denoted by PPT BE$_{all}$ (PPT BE$_X$).

For instance, for $N = 6$, the different possibilities are PPT BE$_1$ (PPT BE across the bipartition 5|1), PPT BE$_2$ (across the bipartition 4|2), PPT BE$_3$ (across the bipartition 4|2), and four combinations of them: PPT BE$_{1,2}$ (across the bipartitions 5|1 and 4|2), PPT BE$_{1,3}$ = PPT BE$_X$ (across the bipartitions 5|1 and 3|3), PPT BE$_{2,3}$ (across the bipartitions 4|2 and 3|3), and PPT BE$_{1,2,3}$ = PPT BE$_{all}$ (across the bipartitions 5|1, 4|2, and 3|3).

We observe that out of all possible bipartitions, there is a nonzero probability of obtaining a RIS with PPT entanglement across only a few. In our example of six qubits out of the seven possible outcomes, there is a nonzero probability of obtaining a RIS with PPT entanglement across only four of them, and as the ancilla parameter increases, their respective probabilities start to increase in a specific order: PPT BE$_1$, PPT BE$_{1,2}$, PPT BE$_{1,2,3}$, and finally, PPT BE$_{1,3}$. These refinements can be observed in Figs. 3 and 4.

Generally, for an N-qubit system, as the ancilla parameters grow, the PPT bound entanglement emerges progressively across more and more bipartitions. First appear the PPT BE$_1$ states, then the PPT BE$_{1,2}$ states, PPT BE$_{1,2,3}$ states, and so on, until the PPT BE$_{all}$ states, and finally the PPT BE$_X$ states. It occurs with a lower probability than PPT BE$_{all}$, and does not behave similarly for every N, nor for the two methods. Indeed, $N = 4$ is the only case where PPT BE$_X$ RIS are more likely to appear than PPT BE$_{all}$ RIS in both methods. Moreover, the probability of PPT BE$_X$ is dramatically smaller (close to 0) for odd numbers than for even numbers N. In Method II, the probability of PPT BE$_X$ tends towards 0 for odd numbers. Another difference between odd and even N can be observed in the growth of the maximal probability of PPT BE$_{all}$ with respect to N as depicted in both Figs. 3 and 4. Indeed, in both methods, the maximal probability increases from $N = 4$ to $N = 5$, but then decreases from $N = 5$ to $N = 6$, and increases again from $N = 6$ to $N = 7$, and so on, displaying a sawtooth behavior. Different behaviors between odd and even number qubits in symmetric qubits systems were also observed in other works [39].

The range of the ancilla parameters d_a and N_a for which there is the highest probability of obtaining PPT bound entanglement increases with the number of qubits N. By identifying the intersection points of the probability curves for distinct entanglement "phase" (NPT, PPT BE, and SEP) as a function of the ancilla parameter N_a for each system size N, one can map out the dominant regimes of each phase. These intersections, extracted from Fig. 3, define the boundaries in the resulting phase diagram (Fig. 5). Notably, the transition from NPT to PPT exhibits a linear dependence on $\sim N$, whereas the

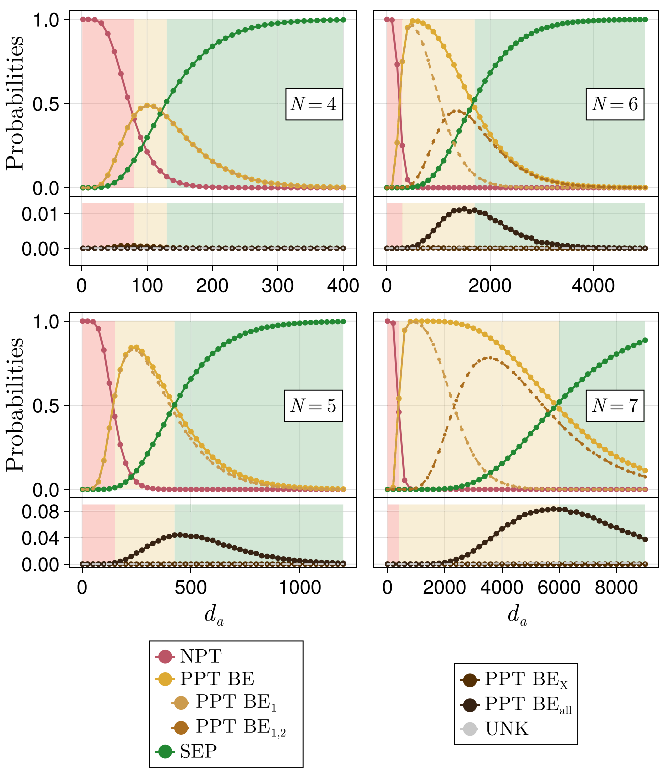

FIG. 4. Bound entanglement in Method II. Probabilities that the generated random induced states have NPT entanglement (red), PPT bound entanglement (yellow), or are separable (green) using Method II with respect to the dimension of the ancilla qudit d_a for $N = 4, \ldots, 7$. The value of the ancilla starts at $d_a = 2$ for each N. For $N = 4, \ldots, 7$, the following values of N_a are multiples of 10, 25, 100, and 200, respectively. The brown curves are a refinement of the PPT BE yellow curve. They show the probabilities of obtaining PPT bound entanglement across the different bipartitions: PPT BE_1 and PPT $\mathrm{BE}_{1,2}$ as the ancilla parameter increases. The PPT BE_1 curve and the global PPT BE curve (yellow) are almost identical for $N = 4$ and 5. The bottom frame exhibit the three probabilities of obtaining PPT BE_X, PPT $\mathrm{BE}_{\mathrm{all}}$, and UNK states. The lines between the dotted points are to guide the eye. The background colors indicate the regions where the probability to get NPT entanglement (red), PPT bound entanglement (yellow), or separable states (green) is the highest compared to the other two.

transition from entanglement to full separability follows a quadratic scaling $\sim N^2$. This scaling behavior highlights that the regime in which bound entanglement can occur grows with N^2, underscoring its increasing relevance in larger systems.

B. Hilbert-Schmidt distance and variety of PPT BE RIS

With the help of the Hilbert-Schmidt (HS) distance, we investigate here the variety of PPT BE RIS generated using the two methods. The Hilbert-Schmidt distance is defined between two operators A and B as $D_{\mathrm{HS}}(A, B) = \sqrt{\mathrm{Tr}[(A-B)^\dagger (A-B)]}$. We first determine the mean distance between random induced states and the maximally mixed state

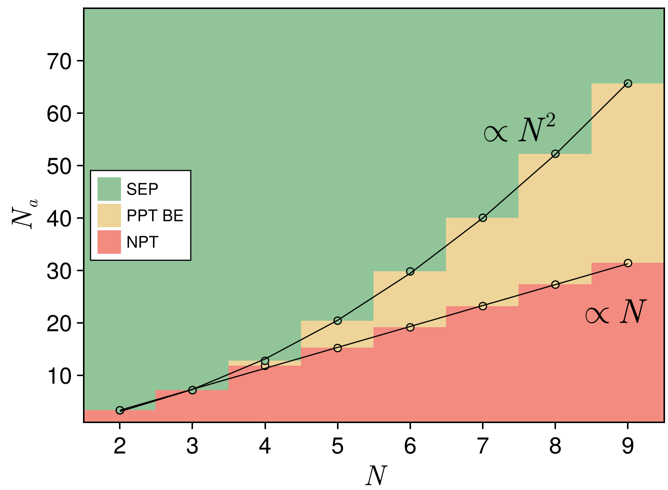

FIG. 5. Entanglement phase diagram. Diagram highlighting where NPT (red), PPT BE (orange), and SEP (green) RIS are the most likely obtained for Method I, as a function of N and N_a. The boundaries correspond to the intersections between the probability curves of Fig. 3. The lines are linear and quadratic fits of the intersection points.

(MMS) ρ_0 in the symmetric subspace

$$\rho_0 = \frac{1}{N+1} \sum_{m=0}^{N} |D_N^{(\alpha)}\rangle\langle D_N^{(\alpha)}| = \frac{\mathbb{1}_{N+1}}{N+1}, \tag{3}$$

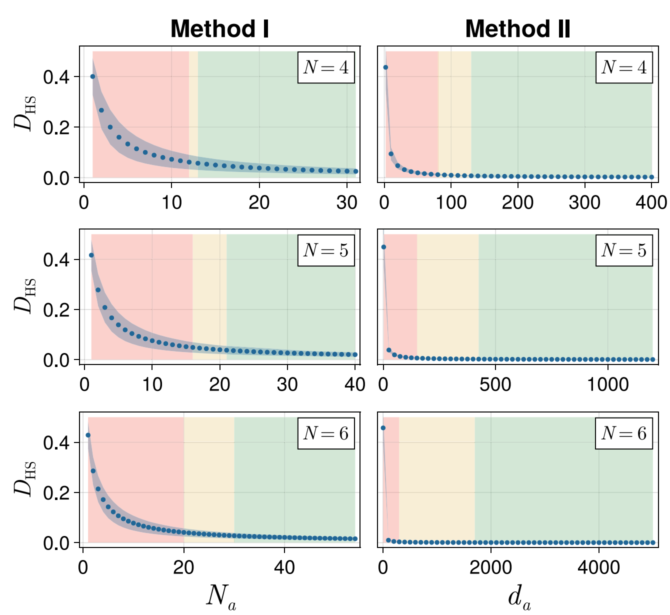

FIG. 6. Mean HS distance in RIS. Mean Hilbert-Schmidt distance D_{HS} between the RIS and the maximally mixed state for $N = 4, 5, 6$ as a function of the ancilla parameter (N_a or d_a) for both methods MI and MII. For each parameter of the ancilla, 100 000 RIS were generated. The lighter blue band indicates the standard deviation, and is continuous to guide the eye. The background colors indicate the regions where the probability of obtaining NPT entanglement (red), PPT bound entanglement (yellow), or separable states (green) is the highest compared to the other two.

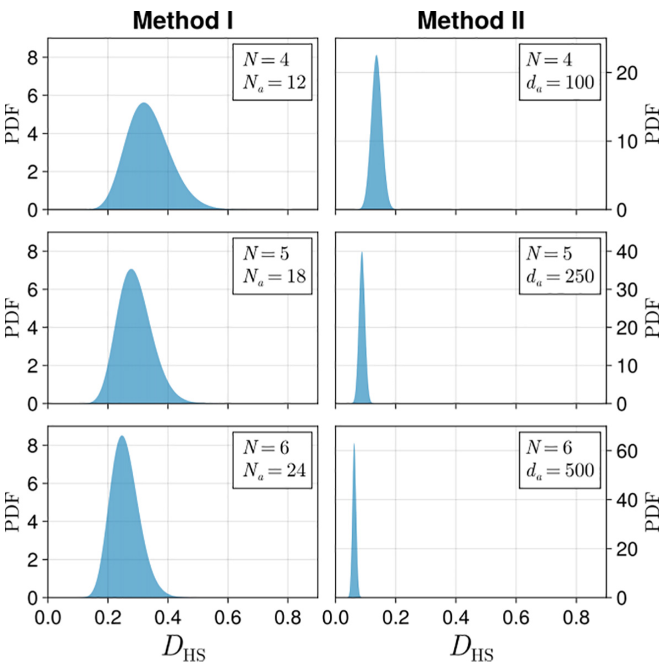

FIG. 7. Variety of bound entangled RIS. PDFs of the Hilbert-Schmidt distance between two random induced bound entangled states using both methods MI and MII (and considering a set of three distinct parameters for each method, see insets). The comparison of the graphs shows that Method I presents a larger variety of bound entangled states than Method II.

with purity $\mathrm{tr}(\rho_0^2) = 1/(N+1)$. Figure 6 depicts how the mean distance for MII decreases dramatically faster to 0 than for MI, for $N = 4, 5, 6$. The yellow background in the panels indicates where the probability of obtaining PPT BE states is the highest compared to the probability of obtaining NPT or SEP RIS. These observations indicate that MII creates bound entangled states much closer to the MMS compared to MI. The same behavior is observed for other numbers N in both methods. Note that $D_{\mathrm{HS}}(\rho_S, \rho_0)$ is directly linked to the purity of the RIS ρ_S: $D_{\mathrm{HS}}(\rho_S, \rho_0) = \mathrm{tr}(\rho_S^2) - 1/(N+1)$. Hence, up to a constant the curves of Fig. 6 also represent the evolution of the mean purity in the RIS w.r.t. the ancilla parameters. We then investigate the variety of the created random induced bound entangled states. To that end, we create samples of random induced PPT BE states of $N = 4$, 5, and 6 qubits using both methods. The ancilla parameters are fixed around the ones giving the maximum probability to get a bound entangled state. For Method I, the selected parameters are $N_a = 12$, 18, and 24 for $N = 4$, 5, and 6, respectively, and $d_a = 100$, 250, and 300 for Method II. Figure 7 displays the probability density functions (PDFs) of the HS distance between two PPT BE RIS for these selected parameters. The PDFs are estimated from a sample of 30 000 bound entangled RIS that generate a sample of $(30\ 000^2 - 30\ 000)/2 = 449\ 985\ 000$ relative distances. In Fig. 8, we show the PDFs of the HS distance between PPT BE RIS of $N = 4$ qubits and the Dicke dyadic products $|D_N^\alpha\rangle\langle D_N^\beta|$ $(\alpha, \beta = 0, \ldots, N)$. These latter PDFs are estimated from a sample of 10^5 bound entangled RIS. The figure shows how the two methods generate bound entangled RIS distributed around the maximally mixed state. The distribution is narrower around the MMS for Method II than for Method I.

C. Comparative analysis of methods I and II

The results presented in the previous section shed light on the distinct features of the two methods for generating PPT BE states. First, for a fixed number of qubits N, and in particular for $N = 4$, 5, and 6, Method I attains a slightly lower maximal probability of producing a PPT BE states than Method II. However, as N increases, this difference becomes negligible, and both methods converge toward nearly identical maximal probabilities close to unity.

A striking difference arises in the range of the control parameter over which PPT BE states are observed with high probability. MII possesses a considerably wider parameter region in which the probability of finding PPT BE states exceeds that of NPT or SEP ones. This broad stability means that MII is less sensitive to parameter variations, offering a more robust performance that could facilitate experimental implementation. The ability to maintain a high generation probability over an extended parameter range may prove advantageous in practical situations where fine control of the ancilla parameter is difficult to achieve.

Conversely, MI exhibits a pronounced advantage in terms of the diversity of the generated states. The ensemble of PPT BE states obtained from MI is significantly more varied as shown in Figs. 7 and 8. This enhanced diversity may be important for theoretical studies aiming to characterize the structure, geometry, or classification of bound entanglement, or for applications requiring an heterogeneous sample of entangled states.

Taken together, these observations suggest that the choice between MI and MII depends on the intended application. If one prioritizes variety and seeks to probe the richness of the PPT BE landscape, MI constitutes the preferred option. If instead the goal is to achieve higher generation probabilities and to benefit from greater robustness to parameter fluctuations (features especially relevant in experimental contexts) MII should be favored. For larger system sizes, where both methods reach nearly maximal probabilities, this distinction becomes less critical; however, in the low-N regime, it remains a significant consideration.

V. CONCLUSION

In this work, we showed that symmetric RIS offered a practical and efficient route to generating bound entangled states, even in low-dimensional systems, as long as the number of qubits satisfied $N > 3$. By considering two distinct methods for generating RIS, namely, partial tracing of symmetric multiqubit pure states (method MI) and tracing out a qudit ancilla (method MII), we demonstrated that bound entanglement emerged naturally for suitable choices of the ancilla parameters. The probabilities of generating such PPT bound entangled states increased rapidly with the system size, reaching values close to unity, thus providing a highly efficient mechanism for producing large ensembles of bound entangled states without complex optimization procedures.

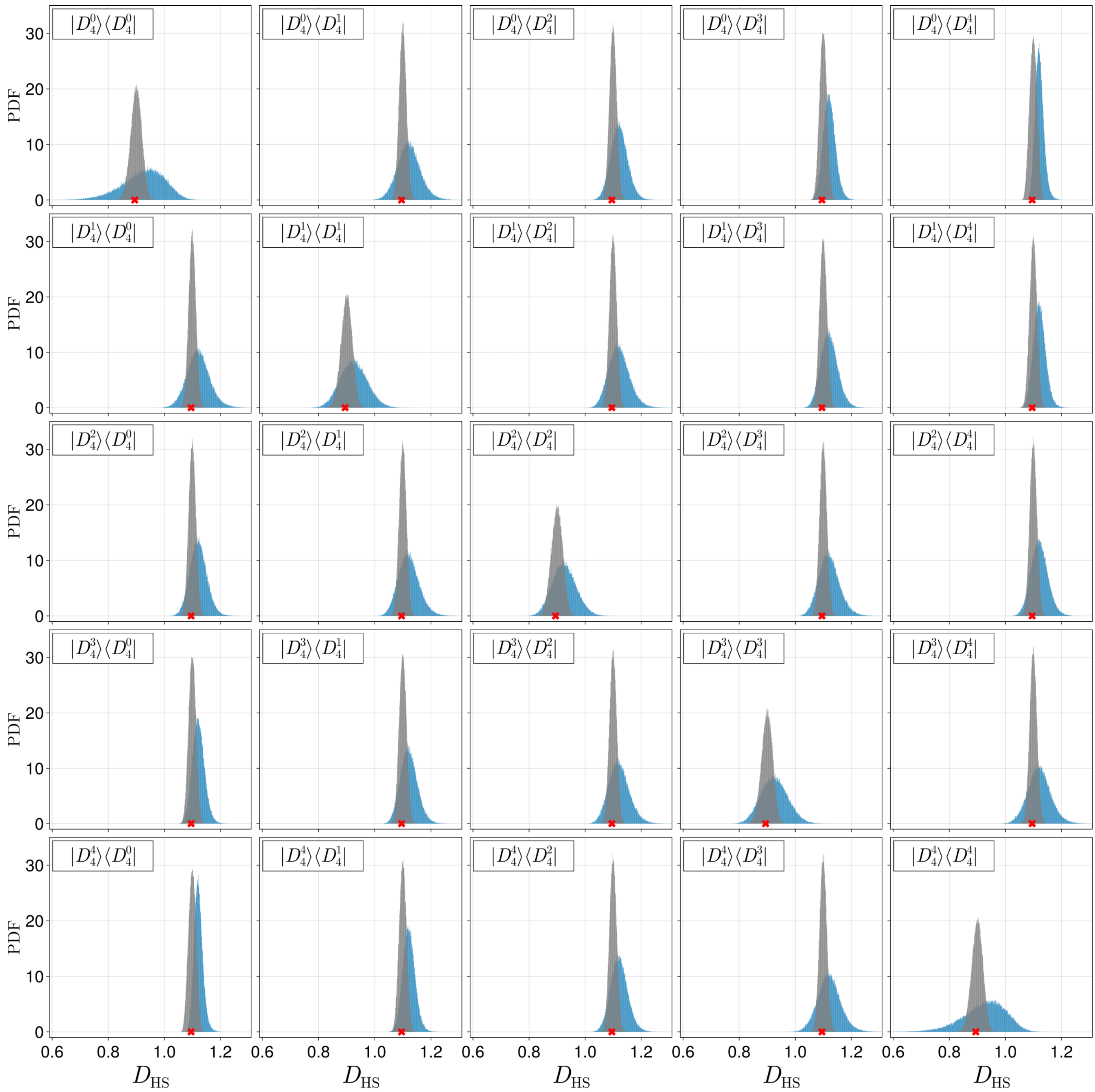

FIG. 8. Spreading of bound entangled RIS. PDFs of the HS distance D_{HS} between a bound entangled RIS and the Dicke dyadic products $|D_N^\alpha\rangle\langle D_N^\beta|$ ($\alpha, \beta = 0, \dots, N$) for $N = 4$, $N_a = 12$ (MI, blue) and $d_a = 80$ (MII, gray). In each graph, the red cross indicates the HS distance between the maximally mixed state ρ_0 and the corresponding Dicke dyadic product.

The results presented here highlight notable patterns in the distribution of PPT bound entanglement across bipartitions, including a sawtooth behavior in the maximal PPT $\mathrm{BE}_{\mathrm{all}}$ probability for odd versus even numbers of qubits and the sequential appearance of PPT entanglement across increasing subsets of bipartitions. Such insights deepen our understanding of multipartite symmetric entanglement and its intricate structure. Furthermore, our exploration of the Hilbert-Schmidt distances provides a quantitative characterization of the diversity of the generated states, illustrating the versatility of symmetric RIS as a resource for entanglement studies.

Our comparative analysis of the two methods reveals a complementary picture. Method I produces a broader variety of bound entangled states, which is valuable for theoretical studies aimed at exploring the structure and geometry of entanglement. Conversely, Method II yields states that are more concentrated around the maximally mixed state, providing higher robustness and a wider parameter range where bound entanglement occurs, which may be advantageous for

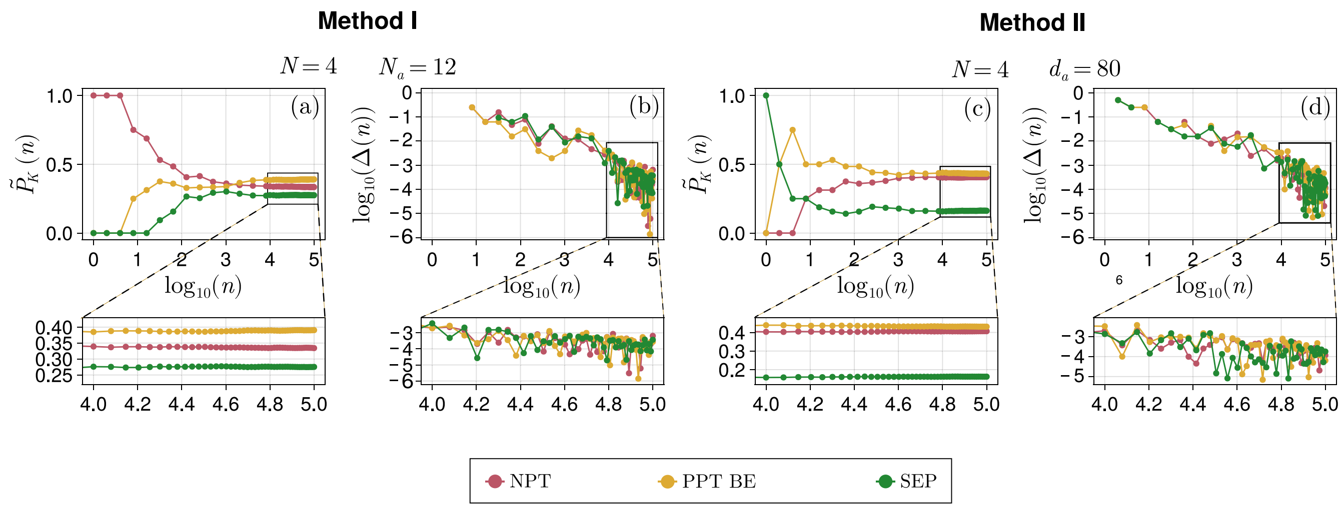

FIG. 9. Empirical probabilities. (a), (c) Empirical probabilities $\tilde{P}_K(n)$ (K = NPT, PPT BE, and SEP) with respect to the number n of RIS generated for $N = 4$ for (a) Methods I and (c) II. The ancilla parameters are $N_a = 12$ for Method I and $d_a = 80$ for Method II. The plot points represent the empirical probabilities computed for the sequence of sample numbers $n = 1, 2, 4, 8, \dots, 8192$ and then from $n = 10^4$ to 10^5 by constant steps of 2000 (continuous lines are only guides for the eyes). (b), (d) Absolute values of the successive differences of the plot points: $\Delta(n_i) = \tilde{P}_K(n_i) - \tilde{P}_K(n_{i-1})$, with i indexing the successive plot points for Methods (b) I and (d) II. The lower four panels display a zoom in the region $n \in [10^4, 10^5]$.

experimental implementations. These distinctions underscore the importance of selecting a method according to the intended application, whether it be for fundamental research, entanglement characterization, or experimental realizations.

Looking forward, our study opens multiple avenues for future research. One promising line of inquiry is to explore the operational utility of the RIS in quantum information processing, metrology, and quantum communication protocols using both methods. Additionally, extending this approach to higher-dimensional systems and other symmetry classes could further enrich the toolkit for the generation and characterization of bound entanglement.

Overall, our work establishes symmetric RIS as a flexible and powerful framework for the generation of bound entangled states, bridging theoretical analysis and potential experimental realization. The combination of high probability generation, controllable state properties, and methodological simplicity positions this approach as a valuable resource for the ongoing exploration of the subtle phenomenon of bound entanglement in quantum systems.

ACKNOWLEDGMENTS

J.L. thanks Eduardo Serrano-Ensástiga, Jérôme Denis, and Thomas Michel for fruitful discussions. T.B. acknowledges financial support from the Fonds de la Recherche Scientifique de Belgique (F.R.S.-FNRS) under grant IISN 4.4512.08. Computational resources were provided by the Consortium des Equipements de Calcul Intensif (CECI), funded by the Fonds de la Recherche Scientifique de Belgique (F.R.S.-FNRS) under Grant No. 2.5020.11.

DATA AVAILABILITY

The data that support the findings of this article are not publicly available upon publication because it is not technically feasible and/or the cost of preparing, depositing, and hosting the data would be prohibitive within the terms of this research project. The data are available from the authors upon reasonable request.

APPENDIX: EMPIRICAL PROBABILITIES

Figure 9 displays the empirical probabilities $\tilde{P}_K(n)$ (K = NPT, PPT BE, and SEP) with respect to the number n of RIS generated for $N = 4$, $N_a = 12$ (Method I) and $d_a = 80$ (Method II). At $n = 10^5$, the empirical probabilities are expected to yield an approximation of the exact probabilities to within a precision of 10^{-3}.

[1] R. Horodecki, P. Horodecki, M. Horodecki, and K. Horodecki, Quantum entanglement, Rev. Mod. Phys. **81**, 865 (2009).

[2] O. Gühne and G. Tóth, Entanglement detection, Phys. Rep. **474**, 1 (2009).

[3] A. Peres, Separability criterion for density matrices, Phys. Rev. Lett. **77**, 1413 (1996).

[4] M. Horodecki, P. Horodecki, and R. Horodecki, Separability of mixed states: Necessary and sufficient conditions, Phys. Lett. A **223**, 1 (1996).

[5] M. Horodecki, P. Horodecki, and R. Horodecki, Mixed-state entanglement and distillation: Is there a "bound" entanglement in nature? Phys. Rev. Lett. **80**, 5239 (1998).

[6] S. Ishizaka, Bound entanglement provides convertibility of pure entangled states, Phys. Rev. Lett. **93**, 190501 (2004).

[7] K. Horodecki, L. Pankowski, M. Horodecki, and P. Horodecki, Low-dimensional bound entanglement with one-way distillable cryptographic key, IEEE Trans. Inf. Theory **54**, 2621 (2008).

[8] G. Tóth and T. Vértesi, Quantum states with a positive partial transpose are useful for metrology, Phys. Rev. Lett. **120**, 020506 (2018).

[9] K. F. Pál, G. Tóth, E. Bene, and T. Vértesi, Bound entangled singlet-like states for quantum metrology, Phys. Rev. Res. **3**, 023101 (2021).

[10] P. Horodecki, Separability criterion and inseparable mixed states with positive partial transposition, Phys. Lett. A **232**, 333 (1997).

[11] P. Horodecki, M. Horodecki, and R. Horodecki, Bound entanglement can be activated, Phys. Rev. Lett. **82**, 1056 (1999).

[12] C. H. Bennett, D. P. DiVincenzo, T. Mor, P. W. Shor, J. A. Smolin, and B. M. Terhal, Unextendible product bases and bound entanglement, Phys. Rev. Lett. **82**, 5385 (1999).

[13] S. Halder and R. Sengupta, Construction of noisy bound entangled states and the range criterion, Phys. Lett. A **383**, 2004 (2019).

[14] L. Skowronek, Three-by-three bound entanglement with general unextendible product bases, J. Math. Phys. **52**, 122202 (2011).

[15] D. P. DiVincenzo, T. Mor, P. W. Shor, J. A. Smolin, and B. M. Terhal, Unextendible product bases, uncompletable product bases and bound entanglement, Commun. Math. Phys. **238**, 379 (2003).

[16] P. Bej and S. Halder, Unextendible product bases, bound entangled states, and the range criterion, Phys. Lett. A **386**, 126992 (2021).

[17] S. Bandyopadhyay, S. Ghosh, and V. Roychowdhury, Non-full-rank bound entangled states satisfying the range criterion, Phys. Rev. A **71**, 012316 (2005).

[18] P. Caban and B. C. Hiesmayr, Bound entanglement is not Lorentz invariant, Sci. Rep. **13**, 11189 (2023).

[19] R. Augusiak, J. Grabowski, M. Kuś, and M. Lewenstein, Searching for extremal PPT entangled states, Opt. Commun. **283**, 805 (2010).

[20] S. Halder, M. Banik, and S. Ghosh, Family of bound entangled states on the boundary of the peres set, Phys. Rev. A **99**, 062329 (2019).

[21] W. Cheng and F. Xu, A general scheme for construction of bound entangled states by convex linear combination, in *2010 IEEE International Conference on Information Theory and Information Security* (IEEE, New York, 2010), pp. 434–437.

[22] A. Rutkowski and M. Studziński, A class of PPT entangled states arbitrary far from separable states, arXiv:1906.10023.

[23] M. Piani and C. E. Mora, Class of positive-partial-transpose bound entangled states associated with almost any set of pure entangled states, Phys. Rev. A **75**, 012305 (2007).

[24] H. Zhao, S. Guo, N. Jing, and S. Fei, Construction of bound entangled states based on permutation operators, Quantum Info. Proc. **15**, 1529 (2015).

[25] P. Badziag, K. Horodecki, M. Horodecki, J. Jenkinson, and S. J. Szarek, Bound entangled states with extremal properties, Phys. Rev. A **90**, 012301 (2014).

[26] J. Tura, R. Augusiak, P. Hyllus, M. Kuś, J. Samsonowicz, and M. Lewenstein, Four-qubit entangled symmetric states with positive partial transpositions, Phys. Rev. A **85**, 060302(R) (2012).

[27] C. Popp and B. C. Hiesmayr, Almost complete solution for the NP-hard separability problem of bell diagonal qutrits, Sci. Rep. **12**, 12472 (2022).

[28] W. Li, R. Han, J. Shang, H. K. Ng, and B.-G. Englert, Sampling quantum states with inequality constraints, arXiv:2109.14215.

[29] E. Sindici and M. Piani, Simple class of bound entangled states based on the properties of the antisymmetric subspace, Phys. Rev. A **97**, 032319 (2018).

[30] L. Clarisse, Construction of bound entangled edge states with special ranks, Phys. Lett. A **359**, 603 (2006).

[31] J. Moerland, N. Wyderka, H. Kampermann, and D. Bruß, Bound entangled bell diagonal states of unequal local dimensions, and their witnesses, Phys. Rev. A **109**, 012217 (2024).

[32] F. Ozaydin, C. Bayindir, A. A. Altintas, and C. Yesilyurt, Nonlocal activation of bound entanglement via local quantum zeno dynamics, Phys. Rev. A **105**, 022439 (2022).

[33] F. Ozaydin, V. Bayrakci, A. A. Altintas, and C. Bayindir, Superactivating bound entanglement in quantum networks via quantum zeno dynamics and a novel algorithm for optimized zeno evolution, Appl. Sci. **13**, 791 (2023).

[34] G. Aubrun, S. J. Szarek, and D. Ye, Entanglement thresholds for random induced states, Commun. Pure Appl. Math. **67**, 129 (2013).

[35] E. Knill, Open quantum problems, https://oqp.iqoqi.oeaw.ac.at/undistillability-implies-ppt.

[36] G. Aubrun, Partial transposition of random states and non-centered semicircular distributions, Random Matrices: Theory Appl. **01**, 1250001 (2012).

[37] K. Życzkowski, K. A. Penson, I. Nechita, and B. Collins, Generating random density matrices, J. Math. Phys. **52**, 062201 (2011).

[38] F. Bohnet-Waldraff, D. Braun, and O. Giraud, Entanglement and the truncated moment problem, Phys. Rev. A **96**, 032312 (2017).

[39] J. Louvet, E. Serrano-Ensástiga, T. Bastin, and J. Martin, Nonequivalence between absolute separability and positive partial transposition in the symmetric subspace, Phys. Rev. A **111**, 042418 (2025).